Available online at www.sciencedirect.com
SCIENCE DIRECT®
ELSEVIER
Mathematics and Computers in Simulation 66 (2004) 255–265
MATHEMATICS AND COMPUTERS IN SIMULATION
www.elsevier.com/locate/matcom

Inverse Dirichlet problem and conformal mapping

R. Kress*

Institut für Numerische und Angewandte Mathematik, Universität Göttingen, Lotzestr. 16-18, 37083 Göttingen, Germany

Available online 16 March 2004

Abstract

In this exposition we consider an inverse Dirichlet problem for harmonic functions that arises in the mathematical modelling of electrostatic imaging methods. In the first part we will survey the main ideas of some reconstruction procedures that have been employed for the numerical solution of this nonlinear and ill-posed inverse boundary value problem. In the second part we will outline a recently developed method that is based on conformal mapping techniques. By some numerical examples we will illustrate the feasibility of this new method.

Keywords: Inverse Dirichlet problem; Conformal mapping; Laplace equation

1. The inverse boundary value problem

The mathematical modelling of electrostatic imaging methods in nondestructive testing and evaluation leads to inverse boundary value problems for the Laplace equation. In principle, in these applications an unknown inclusion within a conducting host medium with constant conductivity is assessed from overdetermined Cauchy data on the accessible part of the boundary of the medium. For simplicity of our presentation, we assume that D is a doubly connected domain in $\mathbb{R}^2$ with the boundary ∂D consisting of two disjoint closed curves Γ_0 and Γ_1 such that Γ_0 is contained in the interior of Γ_1. In electrostatic imaging methods the boundary shape Γ_0 is assessed by imposing a voltage pattern at a number of electrodes attached to the boundary Γ_1 and measuring the resulting currents through the electrodes. In principle, we can distinguish three types of boundary conditions. The determination of the unknown shape Γ_0 of a perfectly conducting inclusion leads to an inverse Dirichlet boundary value problem. The case of a nonconducting inclusion is governed by a Neumann boundary condition and the case of an inclusion with a conductivity that is different from the conductivity of the surrounding background medium D leads to an inverse transmission problem.

* Tel.: +49-55-139-4511; fax: +49-55-139-3944.
E-mail address: kress@math.uni-goettingen.de (R. Kress).
URL: http://www.num.math.uni-goettingen.de/kress/.

0378-4754/$30.00
doi:10.1016/j.matcom.2004.02.006

In this survey we will restrict ourselves to the case of the Dirichlet condition. For a given function f on Γ_1 consider the Dirichlet problem for a function $u \in C^2(D) \cap C(\bar{D})$ satisfying the Laplace equation

$$\Delta u = 0 \quad \text{in } D \tag{1.1}$$

and the boundary conditions

$$u = 0 \quad \text{on } \Gamma_0 \tag{1.2}$$

and

$$u = f \quad \text{on } \Gamma_1. \tag{1.3}$$

The inverse problem we are concerned with is: Given the Dirichlet data f on Γ_1 with $f \neq 0$, i.e., an imposed voltage on the accessible exterior boundary Γ_1 of the conducting medium, and the Neumann data

$$g := \frac{\partial u}{\partial \nu} \quad \text{on } \Gamma_1 \tag{1.4}$$

i.e., the resulting currents on Γ_1, determine the shape of the interior boundary Γ_0. Here, by ν we denote the outward unit normal to Γ_1. As opposed to the forward boundary value problem, the inverse problem is nonlinear and ill-posed.

The first question to ask is uniqueness, i.e., is the interior boundary curve Γ_0 uniquely determined by the Cauchy data (1.3)–(1.4) of a solution u to the boundary value problem (1.1)–(1.3).

Theorem 1.1. *Let Γ_0 and $\tilde{\Gamma}_0$ be two closed curves contained in the interior of Γ_1 and denote by u and $\tilde{u}$ the solutions to the Dirichlet problem* (1.1)–(1.3) *for the interior boundaries Γ_0 and $\tilde{\Gamma}_0$, respectively. Assume that $f \neq 0$ and*

$$\frac{\partial u}{\partial \nu} = \frac{\partial \tilde{u}}{\partial \nu} \tag{1.5}$$

on an open subset of Γ_1. Then $\Gamma_0 = \tilde{\Gamma}_0$.

Proof. Denote by Ω_1 the interior of Γ_1 and by Ω_0 and $\tilde{\Omega}_0$ the interior of Γ_0 and $\tilde{\Gamma}_0$, respectively. Then, by Holmgren's uniqueness theorem, from (1.5) we can conclude that $u = \tilde{u}$ in the connected component W of $\Omega_1 \setminus (\Omega_0 \cup \tilde{\Omega}_0)$ that contains the exterior boundary Γ_1. Without loss of generality, we can assume that $W^* := (\Omega_1 \setminus \bar{W}) \setminus \Omega_0$ is nonempty. Then u is defined in W^* since it describes the solution of (1.1)–(1.3) for Γ_0. It is harmonic in W^*, continuous in $\overline{W}^*$, and satisfies the homogeneous boundary condition $u = 0$ on ∂W^*. This boundary condition follows from the observation that each boundary point of W^* either belongs to Γ_0 or to $\partial W \cap \tilde{\Gamma}_0$. For $x \in \Gamma_0$ we have $u(x) = 0$ as a consequence of the boundary condition for u, and for $x \in \tilde{\Gamma}_0$ we have $u(x) = \tilde{u}(x)$ and therefore $u(x) = 0$ as a consequence of the boundary condition for $\tilde{u}$. Now, by the maximum–minimum principle for harmonic functions we can conclude that $u = 0$ in W^* and consequently, by analyticity, $u = 0$ in D. This, finally, contradicts $f \neq 0$ on Γ_1 and the proof is complete. □

2. Reconstruction methods

We now proceed with describing the main ideas of some numerical methods for solving the inverse problem. In a first group of methods the ill-posedness and the nonlinearity of the inverse problem are separated. In a first step the harmonic function u is reconstructed from the given Cauchy data on Γ_1. In the spirit of a method introduced by Kirsch and Kress [14] for inverse obstacle scattering problems, i.e., for inverse boundary value problems for the Helmholtz equation, we assume a priori that enough information is known about the unknown boundary curve Γ_0 so we can place an auxiliary closed curve C_0 in the interior of Γ_0. Then we try to represent u as a single-layer potential with unknown densities φ_1 on Γ_1 and φ_0 on C_0. The given Cauchy data on Γ_1 lead to a system of integral equations for the unknowns φ_0 and φ_1 that is of the first kind with respect to φ_0 and of the second kind with respect to φ_1. The ill-posedness of the equation of the first kind requires stabilization, for example, by Tikhonov regularization. Then in a second step the unknown interior boundary curve is determined as the location where the boundary condition (1.2) is satisfied in some least squares sense. For a detailed description of this method for a slightly different inverse Dirichlet problem for harmonic functions we refer to [17]. A detailed description for inverse obstacle scattering problems can be found in [7].

This method enjoys as advantages its conceptual simplicity and the fact that its numerical implementation does not require a forward solver for the boundary value problem (1.1)–(1.3). As disadvantages we note that this method does not result in high accuracy for the reconstructions and that in the first step the domain in which the linear ill-posed Cauchy problem needs to be solved is unknown. Furthermore there is a gap between the theoretical foundation of the method and the numerical implementation. Whereas the latter usually is done in two steps as described above, for a satisfactory mathematical analysis the two steps must be combined into one optimization problem.

In a second group of methods the inverse boundary value problem is considered as an ill-posed nonlinear operator equation and iterative techniques are employed for its solution. For fixed Dirichlet data f, the solution to the Dirichlet problem (1.1)–(1.3) defines an operator

$$F : \Gamma_0 \mapsto \frac{\partial u}{\partial \nu}\Big|_{\Gamma_1}$$

that maps the interior boundary curve Γ_0 onto the normal derivative of the solution u on the exterior boundary curve Γ_1. In terms of this operator, given g, the inverse boundary value problem consists in solving the operator equation

$$F(\Gamma_0) = g \tag{2.1}$$

for the unknown boundary curve Γ_0. For the approximate solution of (2.1), it seems natural to apply iterative methods based on linearizing (2.1), such as Newton's method. However, since the linearized version of (2.1) inherits the ill-posedness, the Newton iterations need to be regularized. For details on the theoretical foundation and the numerical implementation we refer to [17].

This approach has the advantages that again, in principle, it is conceptually simple and that it leads to highly accurate reconstructions. For numerical evidence in inverse obstacle scattering, for example, we refer to [9,12,16]. However, as disadvantages we note that the numerical implementation requires the forward solution of the Dirichlet problem (1.1)–(1.3) in each step of the Newton iteration and good a priori information for the initial approximation. Furthermore, in the theoretical foundation both the linearization,

i.e., the computation of the derivative of F with respect to Γ_0 (see [17]) and the convergence analysis for the regularized iterations (see [10,20]) are rather involved.

As a third approach to numerically solve the inverse Dirichlet problem we mention the factorization method where the unknown boundary curve Γ_0 is characterized in terms of spectral data, i.e., in terms of the eigenvalues and eigenfunctions of the Dirichet-to-Neumann operator

$$A_{\Gamma_1} : u|_{\Gamma_1} \mapsto \frac{\partial u}{\partial \nu}\Big|_{\Gamma_1} \tag{2.2}$$

that maps the Dirichlet data of the solution u to (1.1)–(1.3) onto its Neumann data. Originally, factorization methods were proposed by Kirsch [13] for inverse obstacle scattering problems. Extensions to inverse boundary value problems for harmonic functions are described in [5,6,8,17–19].

As advantages of the factorization method we note its elegant mathematics and its simple numerical implementation. The method is fast and does not require any a priori information. However, the reconstructions are not of a very high accuracy and, as main drawback, the factorization method needs the full Dirichlet-to-Neumann map, i.e., many pairs of Cauchy data for the numerical implementation, whereas the above methods and the method of the following Section 3, in principle, require only one pair of Cauchy data.

In closing this section, we want to indicate that we did not intend to provide a complete survey on reconstruction methods for inverse boundary value problems in potential theory. Indeed, we admit that our selection is biased to some extend in the sense that the Göttingen inverse problems gang is involved in all of them.

3. Reconstruction via conformal mapping

The basic idea of the method that we will outline in this section is to conformally map the domain D with unknown interior boundary Γ_0 onto an annulus $B := \{z \in \mathbb{C} : \rho < |z| < 1\}$ with two concentric circles $C_0 := \{z \in \mathbb{C} : |z| = \rho\}$ and $C_1 := \{z \in \mathbb{C} : |z| = 1\}$ as boundaries. Denote by $\Psi : B \to D$ a bijective holomorphic function that conformally maps B onto D such that C_0 and C_1 are mapped onto Γ_0 and Γ_1, respectively. In a first step we construct the boundary values $\Psi|_{C_1}$ on C_1 from the given data f and g by solving a nonlinear nonlocal first order ordinary differential equation. Then in the second step we solve an ill-posed Cauchy problem for the holomorphic function Ψ in B and obtain the unknown boundary curve via $\Gamma_0 = \Psi(C_0)$. Here and in the sequel, we identify the Euclidean space $\mathbb{R}^2$ and the complex plane $\mathbb{C}$ in the usual way.

This approach also separates the inverse boundary value problem into a nonlinear and an ill-posed part, however, with the two parts occurring in reversed order as compared to the first group of methods mentioned above. We note that in the second step the domain for the Cauchy problem, i.e., the annulus B is completely known. Again the method is conceptually straightforward and numerical tests illustrate that it leads to accurate reconstructions. However, it certainly suffers from the disadvantage that through the use of holomorphic functions it is restricted to two-dimensional problems whereas all the other methods described above, of course, have extensions to three dimensions. Nevertheless, it is of some practical importance since two-dimensional electrostatic imaging problems actually occur in applications [2–4].

By the conformal mapping theorem, after relating two points on the exterior boundaries, the radius ρ and the holomorphic function Ψ are uniquely determined. Denoting by L the length of Γ_1 we use an L

periodic parametric representation in terms of arc length

$$\Gamma_1 = \{\gamma(s) : s \in [0, L]\}$$

and assume that the orientation is counter-clockwise. Furthermore we parameterize the unit circle $C_1 = \{e^{it} : t \in [0, 2\pi]\}$ in the usual way and normalize Ψ by prescribing $\Psi(1) = \gamma(0)$. Then there exists a strictly monotonically increasing bijective function

$$\varphi : [0, 2\pi] \to [0, L]$$

that maps arc length on C_1 onto arc length on Γ_1. Obviously, since γ is given, knowing φ is equivalent to knowing $\Psi|_{C_1}$.

Denote by A_ρ the Dirichlet-to-Neumann operator as introduced in (2.2) with the domain D replaced by the annulus B with radius ρ. For the solution u to the Dirichlet problem (1.1)–(1.3) in D and the harmonic function $v := u \circ \Psi$ in B let $\tilde{u}$ and $\tilde{v}$ be corresponding conjugate harmonic functions in D and B, respectively. Then, from $\tilde{v} = \tilde{u} \circ \Psi$ we have

$$\frac{\partial \tilde{v}}{\partial t} = \frac{\partial \tilde{u}}{\partial s}\frac{\mathrm{d}s}{\mathrm{d}t} \quad \text{on } C_1$$

and using the Cauchy–Riemann equations we can conclude that

$$\frac{\partial v}{\partial v} = \frac{\partial u}{\partial v}\frac{ds}{dt} \quad \text{on } C_1. \tag{3.1}$$

Consequently

$$\frac{\mathrm{d}\varphi}{\mathrm{d}t} = \frac{A_\rho(f \circ \varphi)}{g \circ \varphi} \tag{3.2}$$

where, in a slight abuse of notations for convenience we assume that the boundary functions f and g are expressed as functions of arc length on Γ_1. Correspondingly, we interpret A_ρ as an operator acting on 2π periodic functions.

An application of Green's integral theorem to the harmonic functions v and

$$w(z) = \ln\frac{\rho}{|z|}, \quad z \neq 0, \tag{3.3}$$

in the annulus B yields

$$\ln\rho \int_{C_1} \frac{\partial \upsilon}{\partial \nu}\,\mathrm{d}t = -\int_{C_1} \upsilon\,\mathrm{d}t.$$

From this, using (3.1) we find the relation

$$\rho = \exp\left(\frac{\int_0^{2\pi} f \circ \varphi\,\mathrm{d}t}{\int_{\Gamma_1} g\,\mathrm{d}s}\right) \tag{3.4}$$

for the radius ρ of the annulus B.

Note that (3.2), together with $\varphi(0) = 0$, cannot be viewed as a conventional initial value problem, since evaluating $A(f \circ \varphi)$ at a point $t \in [0, 2\pi]$ requires the knowledge of φ on the whole interval

$[0, 2\pi]$. In addition, $\varphi(2\pi) = L$ also must be observed. For these reasons the conventional Volterra integral equation techniques for establishing convergence of the corresponding successive approximations are not applicable.

Integrating (3.2) we arrive at the identity

$$L = \int_0^{2\pi} \frac{A(f \circ \varphi)}{g \circ \varphi} \, \mathrm{d}t \tag{3.5}$$

for the boundary map φ. The property $\varphi(2\pi) = L$ is essential to guarantee that $f \circ \varphi$ is a 2π periodic function. In order to ensure that $\varphi(2\pi) = L$ within the successive approximations derived from interpreting (3.2) as a fixed point equation, we need to incorporate the integral on the right hand side of (3.5) into the iteration procedure. To achieve this, by adding (3.5) to (3.2) we observe that φ also satisfies

$$\frac{\mathrm{d}\varphi}{\mathrm{d}t} = \frac{A(f \circ \varphi)}{g \circ \varphi} + \frac{1}{2\pi} \left(L - \int_0^{2\pi} \frac{A(f \circ \varphi)}{g \circ \varphi} \, \mathrm{d}t \right). \tag{3.6}$$

Now starting with $\varphi(t) = Lt/2\pi$ as initial approximation, we perform the successive iterations

$$\rho_m := \exp\left(- \frac{\int_0^{2\pi} f \circ \varphi_m \, \mathrm{d}t}{\int_{\Gamma_1} g \, \mathrm{d}s} \right)$$

$$\frac{\mathrm{d}\varphi_{m+1}}{\mathrm{d}t} := \frac{A_{\rho_m}(f \circ \varphi_m)}{g \circ \varphi_m} + \frac{1}{2\pi} \left(L - \int_0^{2\pi} \frac{A_{\rho_m}(f \circ \varphi_m)}{g \circ \varphi_m} \, \mathrm{d}t \right), \quad \varphi_{m+1}(0) = 0 \tag{3.7}$$

simultaneously for the radii ρ_m and the functions φ_m. For these iterations the following convergence result can be established. For a proof via the contraction mapping principle we refer to Akduman and Kress [1].

Theorem 3.1. *Provided D is a small perturbation of an annulus and the deviation of the Dirichlet data f from a constant is sufficiently small, the successive approximations φ_m defined by* (3.7) *converge to φ in the H^1 $[0, 2\pi]$ norm.*

For the numerical implementation we approximate

$$\varphi_m(t) \approx \varphi_{m,N}(t) = \frac{L}{2\pi} t + \alpha_{m,0} + \sum_{k=1}^{N} [\alpha_{m,k} \cos kt + \beta_{m,k} \sin kt] \tag{3.8}$$

through a trigonometric polynomial. Then, after setting

$$L_m := \frac{1}{2\pi} \left(\int_0^{2\pi} \frac{A_{\rho_m}(f \circ \varphi_{m,N})}{g \circ \varphi_{m,N}} \, \mathrm{d}t - L \right)$$

we find the Fourier coefficients of the update

$$\varphi_{m+1}(t) \approx \varphi_{m+1,N}(t) = \frac{L}{2\pi} t + \alpha_{m+1,0} + \sum_{k=1}^{N} [\alpha_{m+1,k} \cos kt + \beta_{m+1,k} \sin kt]$$

by solving the linear system

$$(g \circ \varphi_{m,N})(t_k)\{\varphi'_{m+1,N}(t_k) + L_m\} = (A_{\rho_m}(f \circ \varphi_{m,N}))(t_k), \quad k = 1, \ldots, K,$$

with equidistant collocation points $t_k := 2k\pi/K$ and $\varphi_{m+1.N}(0) = 0$ by a least squares fit. The Dirichlet-to-Neumann operator we can evaluate either by using the Fourier series arising from the separation of variables solution of (1.1)–(1.3) or by a boundary integral equation solution.

Now, in the second step, knowing the radius ρ and $\Psi|_{C_1} = \gamma \circ \varphi$ we need to solve the Cauchy problem for determining the holomorphic function Ψ in the annulus B from its values on C_1. Expanding in a Fourier series

$$\gamma(\varphi(t)) = \sum_{k=-\infty}^{\infty} b_k \mathrm{e}^{\mathrm{i}kt}$$

we immediately obtain the Laurent series

$$\Psi(z) = \sum_{k=-\infty}^{\infty} b_k z^k \tag{3.9}$$

for Ψ. Then we find the unknown boundary Γ_0 by inserting $z = \rho \mathrm{e}^{\mathrm{i}t}$ into (3.9) as

$$\Gamma_0 = \left\{ \sum_{k=-\infty}^{\infty} b_k \rho^k \mathrm{e}^{\mathrm{i}kt} : 0 \le t \le 2\pi \right\}.$$

The severe ill-posedness of the Cauchy problem is clearly visible, since small errors in the Fourier coefficients b_{-k}, $k \in \mathbb{N}$, will be amplified by the exponentially increasing factors ρ^{-k}. Hence, in the sense of a singular value cut-off (see [17]), we incorporate a regularization by truncating

$$\Gamma_0 \approx \left\{ \sum_{k=-M}^{M} b_k \rho^k \mathrm{e}^{\mathrm{i}kt} : 0 \le t \le 2\pi \right\}. \tag{3.10}$$

Analogous to a singular value cut-off procedure with discrepancy principle, the truncation index M serving as a regularization parameter can be determined as the smallest integer M with the property

$$||\gamma \circ \varphi||^2_{L^2} - 2\pi \sum_{k=-M}^{M} |b_k|^2 \le \delta^2,$$

where δ is some error level for the accuracy of $\gamma \circ \varphi$ as obtained from the first step.

For $f = f_0 =$ constant, using the function w in (3.3), we conclude that

$$A_\rho f_0 = -\frac{f_0}{\ln \rho}$$

and consequently, in this case, the differential Equation (3.2) reads

$$\frac{\mathrm{d}\varphi}{\mathrm{d}t} = -\frac{1}{\ln \rho} \frac{f_0}{g \circ \varphi}. \tag{3.11}$$

Note that (3.11) is local and that, in addition, (3.4) becomes an explicit equation

$$\rho = \exp\left(-\frac{2\pi f_0}{\int_{\Gamma_1} g \, \mathrm{d}s} \right) \tag{3.12}$$

for the radius ρ. This particular case was considered by Idemen and Akduman [11]. However, the above analysis differs from that in [11], since we solve for the boundary map φ by viewing (3.1) as a differential equation whereas the approach in [11] is purely based on complex analysis and restricted to the case where Γ_1 also is a circle.

A further motivation to also allow nonconstant Dirichlet data on Γ_1 is to create the possibility of increasing the accuracy by using more than one pair of Cauchy data for solving the inverse problem. In this case, the boundary function φ has to satisfy the differential Eq. (3.2) for all pairs of Cauchy data. We expect that incorporating this in a least squares sense will lead to an increase in the accuracy and the stability of the reconstructions. Whereas for constant boundary data f the above conformal mapping algorithm cannot work for the inverse Neumann and the inverse transmission problem, we also expect that the more general approach can be extended to these boundary conditions. However, for both the Neumann and the transmission boundary condition the no-flux condition $\int_{\Gamma_1} (\partial u/\partial \nu) \mathrm{d}s = 0$ has to be taken into account. This will require additional considerations and might cause challenging difficulties both from a theoretical and numerical point of view.

4. Numerical examples

We conclude with two numerical examples where, for the sake of simplicity, the exterior boundary curve Γ_1 is chosen as the unit circle. The Cauchy data pair is obtained synthetically by solving the Dirichlet problem via the double-layer potential approach (see [17]). We note, that to obtain uniquely solvable integral equations, the double-layer potential on the interior curve has to be augmented by a suitable single-layer potential. As Dirichlet data in both examples we have chosen the simplest case $f = 1$ on Γ_1.

As a first example we consider the case where Γ_0 is an apple-shaped domain with the parametrization given by

$$\Gamma_0 = \left\{ (-0.3, 0) + \frac{0.6 + 0.54\cos t + 0.06\sin 2t}{1 + 0.75\cos t} (\cos t,\ \sin t) : t \in [0, 2\pi] \right\}.$$

Fig. 1 gives the reconstruction with $M = 16$, $N = 32$, and $K = 64$ using synthetic data that are obtained by a Nyström method with 64 quadrature points on each of the two boundary curves. The radius of the annulus B is obtained as $\rho = 0.6135$. The dashed line represents the exact curve Γ_0 and the full line gives the reconstruction. As to be expected the nonconvex part of Γ_0 is reconstructed not as accurately as the convex part. As mentioned above, at this point it seems worthwhile to investigate whether using more than one Cauchy pair can increase the quality of the reconstructions. Furthermore, different choices for f could also lead to improvements.

To indicate the stability of the method with respect to perturbed data, Fig. 2 gives the reconstruction for 3% random noise added to the data. For regularization in this case we choose the truncation index $M = 8$.

Although the theoretical results in [1] do not include the case of a crack as interior curve Γ_0, in principle, the above ideas also carry over to this limiting case. Here, the reconstructions are not as accurate as in the case of closed curves. More research on the proper regularization is required to enable more satisfactory accuracy. However, it is possible to use the image $\Psi(C_{0,\lambda})$ of the circle

$$C_{0,\lambda} = \{z \in \mathbb{C} : |z| = (1 + \lambda)\rho\}$$

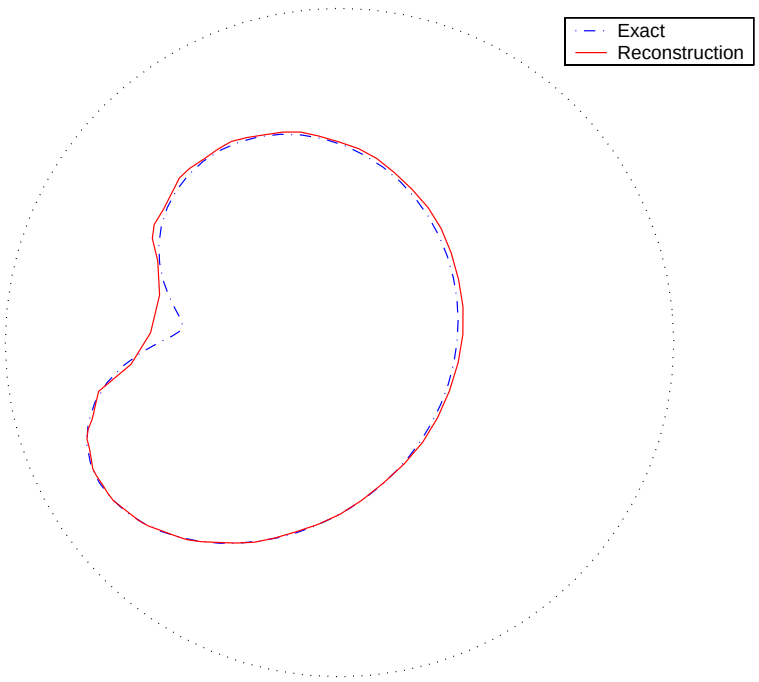

Fig. 1. Exact and reconstructed curves for apple-shaped curve.

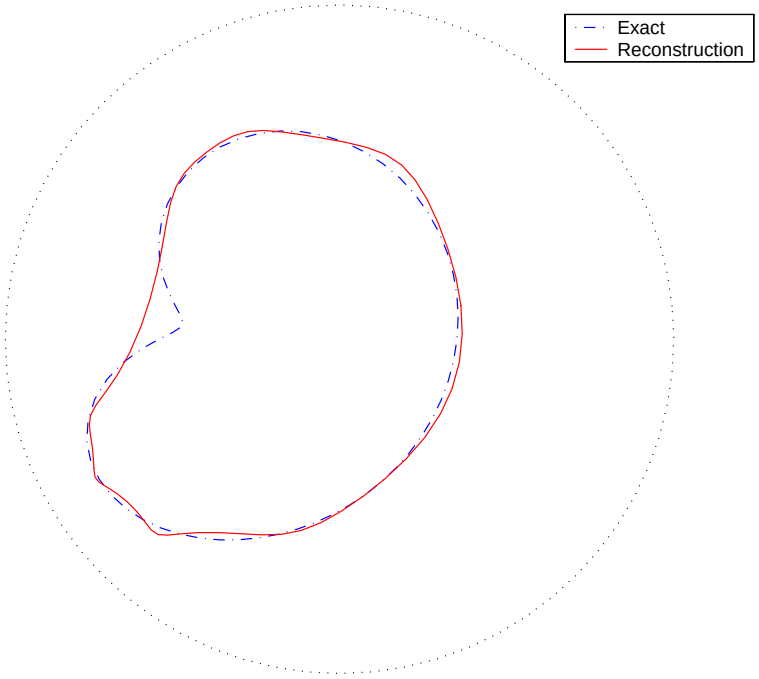

Fig. 2. Exact and reconstructed curves for apple-shaped curve with noisy data.

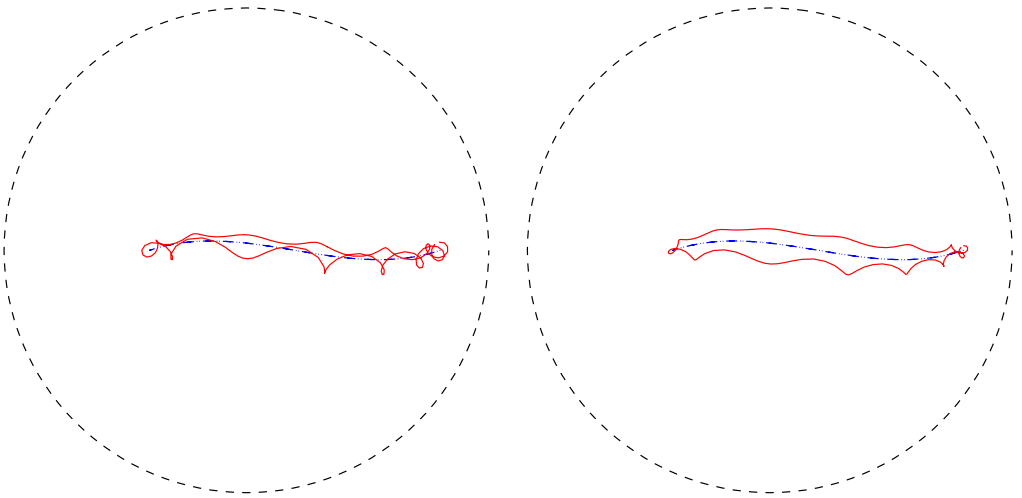

Fig. 3. Exact and reconstructed crack.

with some $\lambda > 0$ to construct a closed curve that contains the unknown crack. From this, for example, initial approximations for Newton type iterations as mentioned in Section 2 could be obtained. We may view λ as an additional regularization parameter. The numerical performance is illustrated by considering the crack with the parametric representation

$$\Gamma_0 = \{x(t) = (0.2 + 0.6t, 0.1t(t^2 - 1)), \quad t \in [-1, 1]\}.$$

Here, the synthetic Cauchy data are obtained by solving the Dirichlet problem in a domain with a crack via the double-layer potential approach on Γ_1 combined with the single-layer potential approach on the crack Γ_0. The latter leads to Symm's integral equation that can be efficiently solved numerically via the cosine substitution (see [15]). Here, we used $M = 12$, $N = 32$, and $K = 64$. For creating the synthetic data again 64 quadrature points on both Γ_1 and Γ_0 were used for the discretization of the integral equations. The radius of the annulus B is obtained as $\rho = 0.3306$. Fig. 3 gives the reconstructions for $\lambda = 0.05$ (left) and $\lambda = 0.1$ (right). Again the dashed line represents the exact crack Γ_0 and the full line gives the reconstruction, i.e., approximate domains that include the crack.

References

[1] I. Akduman, R. Kress, Electrostatic imaging via conformal mapping, Inverse Problems 18 (2002) 1659–1672.
[2] H.T. Banks, M.L. Joyner, B. Wincheski, W.P. Winfree, Real time computational algorithms for eddy-current-based damage detection, Inverse Problems 18 (2002) 795–823.
[3] H.T. Banks, F. Kojima, Boundary shape identification in two-dimensional electrostatic problems using SQUIDs, J. Inv. Ill.-Posed Problems 8 (2000) 467–504.
[4] H.T. Banks, F. Kojima, Identification of material damage in twodimensional domains using the SQUID-based nondestructive evaluation system, Inverse Problems 18 (2002) 1831–1855.
[5] M. Brühl, Explicit characterization of inclusions in electrical impedance tomography, SIAM J. Math. Anal. 32 (2001) 1327–1341.
[6] M. Brühl, M. Hanke, Numerical implementation of two noniterative methods for locating inclusions by impedance tomography, Inverse Problems 16 (2000) 1029–1042.

[7] D. Colton, R. Kress, Inverse Acoustic and Electromagnetic Scattering Theory, second ed., Springer-Verlag, Berlin, 1998.
[8] P. Hähner, An inverse problem in electrostatics, Inverse Problems 15 (1999) 961–975.
[9] T. Hohage, Logarithmic convergence rates of the iteratively regularized Gauss-Newton method for an inverse potential and an inverse scattering problem, Inverse Problems 13 (1997) 1279–1299.
[10] T. Hohage, Iterative Methods in Inverse Obstacle Scattering: Regularization Theory of Linear and Nonlinear Exponentially Ill-Posed Problems, Dissertation, Linz 1999.
[11] M. Idemen, I. Akduman, Some geometrical inverse problems connected with two-dimensional static fields, SIAM J. Appl. Math. 48 (1988) 703–718.
[12] A. Kirsch, The domain derivative and two applications in inverse scattering theory, Inverse Problems 9 (1993) 81–96.
[13] A. Kirsch, Characterization of the shape of the scattering obstacle by the spectral data of the far field operator, Inverse Problems 14 (1998) 1489–1512.
[14] A. Kirsch, R. Kress, An optimization method in inverse acoustic scattering, vol. 3, in: Brebbia, et al. (Eds.), Boundary Elements IX, Fluid Flow and Potential Applications, Springer-Verlag, Berlin, 1987, pp. 3–18.
[15] R. Kress, Inverse scattering from an open arc, Math. Meth. Appl. Sci. 18 (1995) 267–293.
[16] R. Kress, Integral equation methods in inverse acoustic and electromagnetic scattering, in: Ingham, Wrobel (Eds.), Boundary Integral Formulations for Inverse Analysis, Computational Mechanics Publications, Southampton, 1997, pp. 67–92.
[17] R. Kress, Linear Integral Equations, second ed., Springer-Verlag, New York, 1999.
[18] R. Kress, Inverse boundary value problems in potential theory, Cubo Mathematica Educacional 3 (2001) 393–414.
[19] R. Kress, L. Kühn, Linear sampling methods for inverse boundary value problems in potential theory, Appl. Numer. Math. 43 (2002) 143–155.
[20] R. Potthast, On the convergence of a new Newton-type method in inverse scattering, Inverse Problems 17 (2001) 1419–1434.